Structural diversity and electronic properties in potassium silicides

Chun-Mei Hao, Yunguo Li, Hong-Mei Huang, and Yan-Ling Li

Articles you may be interested in

Constructing first-principles phase diagrams of amorphous Li_xSi using machine-learning-assisted sampling with an evolutionary algorithm
The Journal of Chemical Physics **148**, 241711 (2018); 10.1063/1.5017661

Silicon clathrates for photovoltaics predicted by a two-step crystal structure search
Applied Physics Letters **111**, 173904 (2017); 10.1063/1.5000444

Neural networks vs Gaussian process regression for representing potential energy surfaces: A comparative study of fit quality and vibrational spectrum accuracy
The Journal of Chemical Physics **148**, 241702 (2018); 10.1063/1.5003074

Learning structure-property relationship in crystalline materials: A study of lanthanide–transition metal alloys
The Journal of Chemical Physics **148**, 204106 (2018); 10.1063/1.5021089

Quantum tunneling of thermal protons through pristine graphene
The Journal of Chemical Physics **148**, 204707 (2018); 10.1063/1.5024317

Guest Editorial: Special Topic on Data-Enabled Theoretical Chemistry
The Journal of Chemical Physics **148**, 241401 (2018); 10.1063/1.5043213

Structural diversity and electronic properties in potassium silicides

Chun-Mei Hao,[1] Yunguo Li,[2] Hong-Mei Huang,[1] and Yan-Ling Li[1,a)]
[1]*School of Physics and Electronic Engineering, Jiangsu Normal University, Xuzhou 221116, China*
[2]*Department of Earth Sciences, University College London, Gower Street, London WC1E 6BT, United Kingdom*

Stable potassium silicides in the complete compositional landscape were systematically explored up to 30 GPa using the variable-composition evolutionary structure prediction method. The results show that K_4Si, K_3Si, K_5Si_2, K_2Si, K_3Si_2, KSi, KSi_2, KSi_3, and K_8Si_{46} have their stability fields in the phase diagram. The spatial dimensional diversity of polymerized silicon atoms (0D "isolated" anion, dimer, Si_4 group, 1D zigzag chain, 2D layer, and 3D network) under the potassium sublattice was uncovered as silicon content increases. Especially, the 2D layered silicon presents interestingly a variety of shapes, such as the "4 + 6" ring, "4 + 8" ring, and 8-membered ring. K-Si bonding exhibits a mixed covalency and ionicity, while Si-Si bonding is always of covalent character. Semiconductivity or metallicity mainly depends on the form of sublattices and K:Si ratio, which allows us to find more semiconductors in the Si-rich side when closed-shell K cations are encompassed by polymerized Si. The semiconducting silicides present strong absorption in the infrared and visible light range. These findings open up the avenue for experimental synthesis of alkali metal-IVA compounds and potential applications as battery electrode materials or photoelectric materials. *Published by AIP Publishing.*
https://doi.org/10.1063/1.5026699

I. INTRODUCTION

The family of alkali metal- and alkaline earth metal-IVA compounds has been attracting considerable attention recently, not only because of their various extraordinary properties and potential applications but also because they can actually be precursors for novel group-IVA allotropes that cannot be prepared in other ways.[1–9] The polymerized behavior of carbon or silicon atoms under the framework of alkali metal and alkaline earth metal under pressure has been widely discussed by combined theoretical and experimental studies.[3–5,10–15] A calcium carbide with a high carbon content could act as a precursor to fabricate a variety of three-dimensional structures of carbon by removing metal atoms.[11,16] This idea has been successfully applied to design novel allotropes of silicon. Using Na_4Si_{24} synthesized in the Na-Si binary system under high pressure, Kim *et al.* prepared an open-framework allotrope of silicon, Si_{24}, a semiconductor with a quasi-direct bandgap.[6] Subsequently, other silicon allotropes were consecutively suggested by removing the guest-free alkali metal atoms theoretically.[17,18] The success in these systems strongly motivates us to further the search and design of new materials in other alkaline metal-IVA systems.

Although there are plenty of theoretical and experimental studies on the Li–Si[8,9,19–31] and Na–Si system,[6,17,18] study on the K–Si system is very limited. For the K–Si system, there are three known phases at ambient conditions: KSi,[32–34] $K_{12}Si_{17}$,[35] and K_8Si_{46}.[36] KSi crystallizes in a cubic KGe-type structure (space group $P\text{-}43n$, 32 molecules per unit cell, i.e., Z = 32), in which both K and Si atoms form tetrahedrons.[32,33] KSi can be written as K_4Si_4 because of the existence of cluster Si_4^{4-}. KSi can absorb hydrogen to form the potassium silanide, $KSiH_3$, a reversible hydrogen storage material.[37] The reported high-pressure form of tetragonal KSi is of the NaPb-type (space group $I4_1/acd$, Z = 32).[34] $K_{12}Si_{17}$ contains isolated Si_9^{4-} clusters and is a potential precursor candidate for silicon clusters in solution.[35] In addition, some studies on the K–Si system focused on exploring the pressure-induced isostructural volume collapse observed during the phase transition of type I silicon-clathrate.[38–40] K_8Si_{46} exhibits an unusual volume collapse transition at about 15 GPa, while apparently retaining the same cubic clathrate crystal structure, which is followed by a pressure-induced amorphization above 32 GPa.[38] The isostructural phase transition and reversible amorphization observed in K_8Si_{46} indicate that there are thermodynamically stable new compounds in the K–Si system. Therefore, it is absolutely necessary to perform a complete phase diagram search for stable compounds in the K–Si system by using fruitful crystal structural prediction methods.

In this work, the thermodynamic phase diagram of the K–Si system in the range of 0–30 GPa is investigated by means of evolutionary algorithm[41,42] in combination with first-principles total energy calculations. To obtain thermodynamically stable stoichiometries, we perform variable composition structural search in the whole compositional space, which has successfully uncovered novel compounds in many systems.[13,43] The thermodynamic stability field of predicted compounds is determined via free energy calculations under harmonic approximation. Besides, electronic structures and bonding characteristics are systematically discussed. We find that the Si-rich compounds are semiconductors, except for

a)ylli@jsnu.edu.cn

Fd-3*m*-KSi$_2$ and *P*-1-KSi, while the K-rich compounds are all metals, except for *P*-1-K$_3$Si$_2$ and *R*-3*m*-K$_4$Si. The *P*-1-K$_3$Si$_2$ and *R*-3*m*-K$_4$Si are semiconductors with an indirect bandgap.

II. COMPUTATIONAL METHODS

Searches for stable structures in the K–Si system under compression were carried out using the evolutionary algorithm USPEX code[41,42] coupled with the Vienna Ab-initio Simulation Package (VASP) program[44] based on density functional theory (DFT) within the generalized gradient approximation with the exchange-correlation functional of Perdew-Burke-Ernzerhof (PBE).[45] The electron-ion interaction was depicted by means of the projector-augmented wave (PAW) with $3p^6 4s^1$ and $3s^2 3p^2$ as valence electrons for K and Si, respectively. The most interesting structures were further relaxed with a basis set cutoff of 350 eV. The enthalpy of formation per atom of K$_n$Si$_m$ is defined as $\Delta H_f(K_n Si_m) = [H(K_n S_m) - nH(K) - mH(Si)]/(n+m)$, where all enthalpies H are given at the same pressure and zero temperature. Phonon calculations were performed to determine the dynamical stability of the predicted structures by using the finite displacement approach as implemented in the Phonopy code.[46,47] The lattice dynamic properties were also checked by the QUANTUM ESPRESSO package[48] using PAW pseudopotentials with a cutoff energy of 50 Ry. The electron localization function (ELF)[49] was used to analyze the chemical bonds.

III. RESULTS AND DISCUSSION

A. Thermodynamic phase diagram

The evolutionary algorithm USPEX,[41,42] which can simultaneously find stable stoichiometries and the corresponding structures in multicomponent systems, was used to predict

stable K–Si compounds and their structures. In these calculations, all stoichiometries were allowed (with the constraint that the total number of atoms in the unit cell being below 32 atoms), and calculations were performed at 5 GPa, 10 GPa, 20 GPa, and 30 GPa. The pressure-composition phase diagram of the K–Si system is given in Fig. 1(a). In our calculations, we also included an identified phase K$_8$Si$_{46}$.[38,39] As shown in Fig. 1(a), the K–Si compounds located on the convex hull are thermodynamically stable against decomposition to any other binaries or the elements, while the compounds above the convex hull are metastable. Consequently, we found that K$_4$Si, K$_3$Si, K$_5$Si$_2$, K$_2$Si, K$_3$Si$_2$, KSi, KSi$_2$, KSi$_3$, and K$_8$Si$_{46}$ have thermodynamic stability fields on the phase diagram: K$_4$Si, stable above 9 GPa; K$_3$Si, stable above 20 GPa; K$_5$Si$_2$, stable above 6.5 GPa to 28.5 GPa; K$_2$Si, stable above 12.5 GPa; K$_3$Si$_2$, stable above 15 GPa to 27.5 GPa; KSi, stable from 0 to 22.5 GPa; KSi$_2$, stable above 18.5 GPa; KSi$_3$, stable from 2.5 to 19.5 GPa; and K$_8$Si$_{46}$, stable from 0 to 17.5 GPa [see Fig. 1(b)]. For all the newly predicted structures, calculated phonon dispersion curves confirmed their dynamical stability (see Fig. 2 and Figs. S2 and S3 of the supplementary material).

As expected, we found that the upper limit of stability domain of K$_8$Si$_{46}$ (~17.5 GPa) agrees well with its isostructural phase transition pressure (~15 GPa) observed experimentally.[38] Therefore, one can conclude that the volume collapse and amorphization of K$_8$Si$_{46}$ are closely related to the change of thermodynamic stability under strong compression. Theoretically, K$_8$Si$_{46}$ decomposed to KSi$_3$ (from 17.5 to 19.0 GPa) and *sH*-silicon (simple hexagonal phase of silicon) or KSi$_2$ (above 20 GPa) and *sH*-silicon above 17.5 GPa.

In addition, we found that some K–Si compounds can undergo a series of structural phase transitions within the considered pressure range [see Fig. 1(b)]. The *P*-1-K$_2$Si
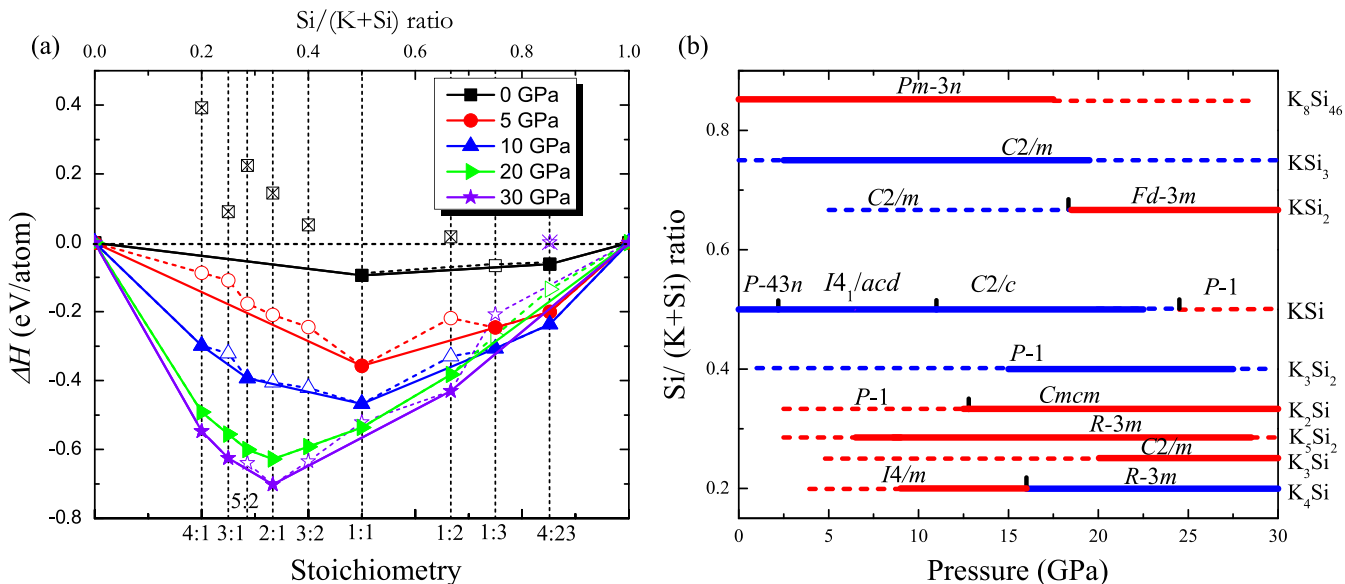

FIG. 1. (a) Convex hull diagram for the K–Si system at examined pressures. (b) Pressure-composition phase diagram of the K–Si system. Thick solid lines represent thermodynamically stable phases and dashed lines represent the metastable ones (red lines represent the metal and blue lines represent the semiconductor).
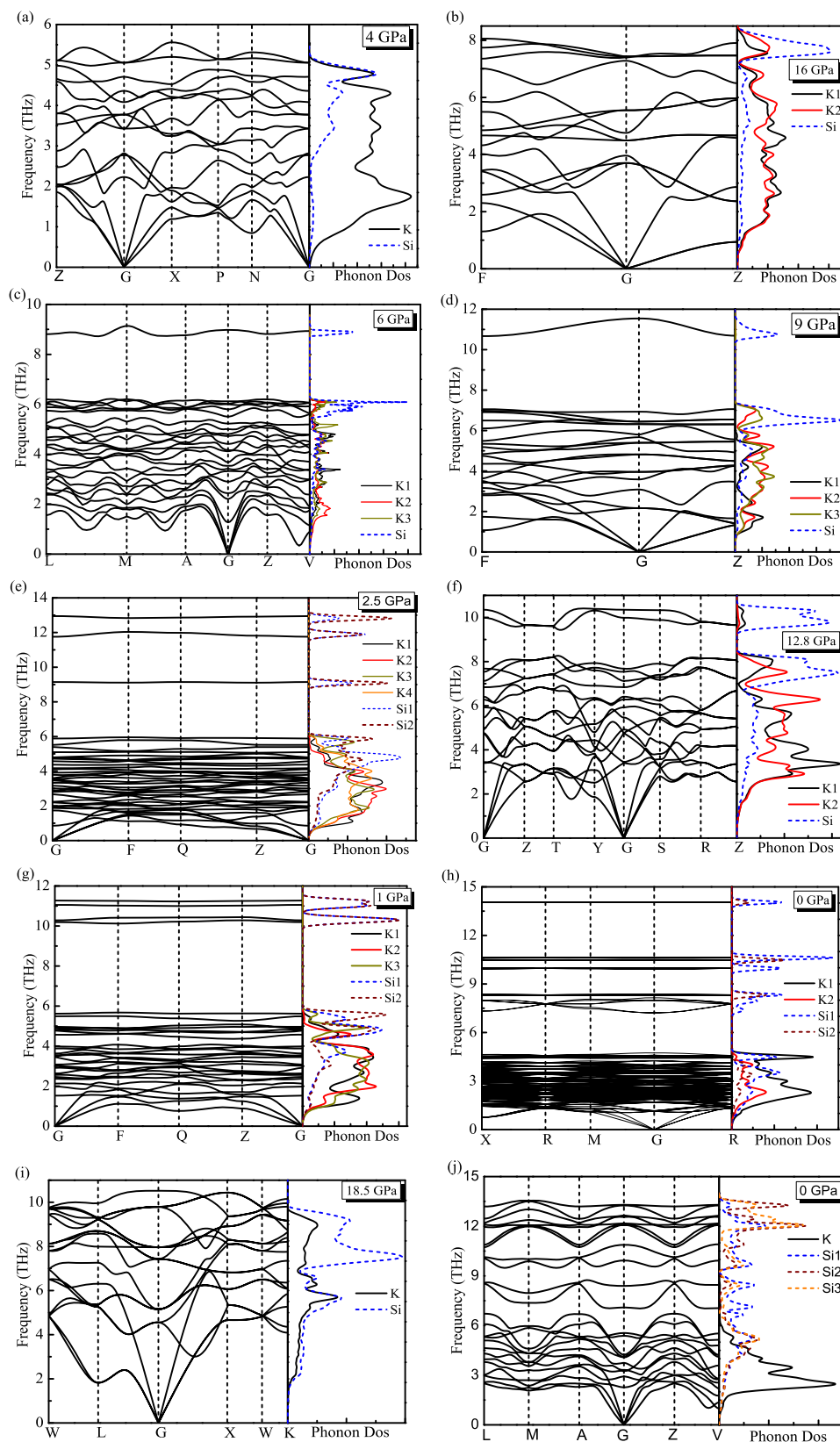
FIG. 2. Phonon dispersion curves and partial atomic phonon density of states (phonon DOSs) of (a) $I4/m$-K_4Si, (b) R-$3m$-K_4Si, (c) $C2/m$-K_3Si, (d) R-$3m$-K_5Si_2, (e) P-1-K_2Si, (f) $Cmcm$-K_2Si, (g) P-1-K_3Si_2, (h) P-$43n$-KSi, (i) Fd-$3m$-KSi_2, and (j) $C2/m$-KSi_3 at examined pressures.

transformed into the orthorhombic $Cmcm$-K_2Si at 12.8 GPa. In the case of KSi, the P-$43n$-KSi transformed to the $I4_1/acd$-KSi at 2.2 GPa and to the $C2/c$–KSi at 11 GPa, followed by the P-1-KSi at 24.5 GPa (see Fig. S1 of the supplementary material). The monoclinic $C2/m$-KSi_2 transformed into the cubic Fd-$3m$-KSi_2 at 18.5 GPa.

B. Dynamical and structural properties

To confirm the dynamical stability of the predicted compounds, we calculated the phonon spectra along the high-symmetry directions in the Brillouin zone (BZ) at corresponding pressures. One can conclude that the predicted compounds

together with the well-known K_8Si_{46} are dynamically stable within their thermodynamic-stability pressure domain since there is no imaginary frequency in the calculated phonon spectra, as shown in Fig. 2 and Figs. S2 and S3 of the supplementary material. From the partial atomic phonon density of states (PHDOSs), Si atoms almost dominate the whole frequency range, but with a slight emphasis relatively on the high-frequency modes, whereas K atoms dominate relatively the low frequency modes because of its relatively large atomic mass. For the K-rich side, including KSi, there are larger frequency gaps in the optical branches part because of the

peculiar polymerization form of silicon atoms (0D, 1D and 2D, see Figs. 2 and 3 and Figs. S2 and S3 of the supplementary material), which in nature originates from the chemical bonding network topology, i.e. links between the Si sublattice and K sublattice. Generally, PHDOS of Si hovers over the high-frequency region if there is direct bonding of covalent character between Si atoms, which propagates into the lower-frequency region if there is abundant direct bonding of ionic character between Si and K or Si is isolated by K.

All stable structures of the K–Si system are plotted in Fig. 3. The equilibrium lattice parameters of the predicted
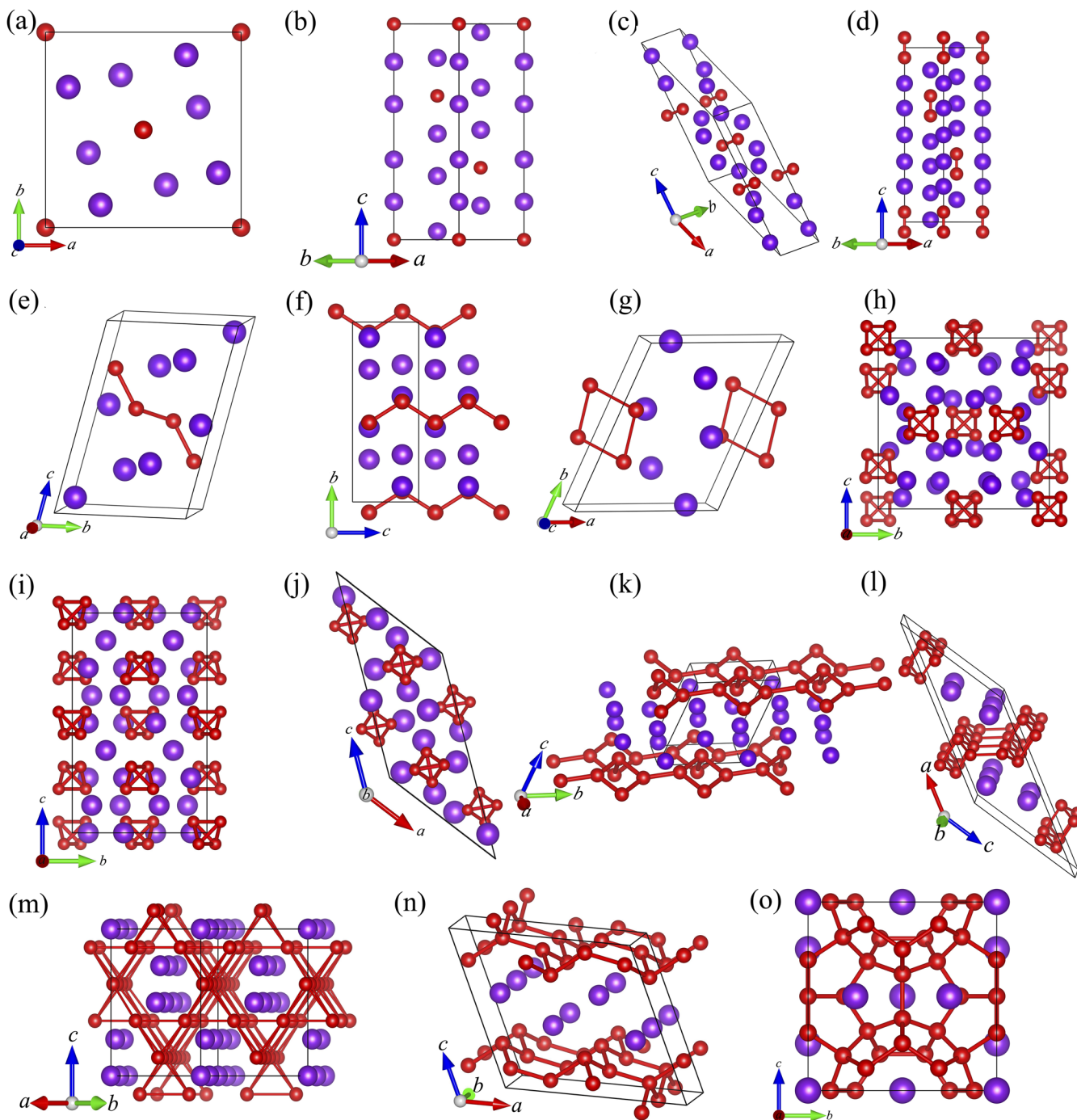

FIG. 3. Crystal structures of K-Si compounds. (a) $I4/m$-K_4Si, (b) R-$3m$-K_4Si, (c) $C2/m$-K_3Si, (d) R-$3m$-K_5Si_2, (e) P-1-K_2Si, (f) $Cmcm$-K_2Si, (g) P-1-K_3Si_2, (h) P-$43n$-KSi, (i) $I4_1/acd$-KSi, (j) $C2/c$-KSi, (k) P-1-KSi, (l) $C2/m$-KSi_2, (m) Fd-$3m$-KSi_2, (n) $C2/m$-KSi_3, and (o) Pm-$3n$-K_8Si_{46}.

phases at examined pressures are given in Table S1 of the supplementary material. We find that the silicon sublattices within all predicted silicide phases have a close correlation with the K:Si ratio (see Fig. 3). Similar to our previous study on the Ca–C system,[3,4,13] the polymerization of silicon atoms underwent great changes with the increasing silicon content; that is, isolated silicon atoms are polymerized, in turn, into Si_2 dumbbells, Si_4 groups, chains, layers, and three-dimensional framework structures (see Figs. 3 and 4). Let us discuss the predicted phases in order of the increasing silicon content.

K_4Si. It is thermodynamically stable (metastable between 4 GPa and 9 GPa) above 9 GPa [space group $I4/m$ (Z = 2)]. The tetragonal K_4Si with $I4/m$ symmetry [see Fig. 3(a)] is thermodynamically stable up to about 16 GPa. The "isolated" Si atoms occupy the crystallographic $2b$ sites, while alkali metal atoms hold $8h$ sites (see Table S1 of the supplementary material). The tetragonal structure of K_4Si has been observed in Li_4C[10] and has also been favored by highly compressed Li_4Si.[31] Above 16 GPa, the semi-metallic $I4/m$-K_4Si gives way to the semiconducting R-$3m$-K_4Si [see Fig. 3(b)], in which the "isolated" Si atom is surrounded by eight K atoms (i.e., eight-fold coordinated silicon).

K_3Si. The monoclinic structure of K_3Si [space group $C2/m$, Z = 4, Fig. 3(c)] is predicted to be thermodynamically stable above 20 GPa (the metastable one between 4.8 and 20 GPa). Both Si atoms and K atoms occupy the $4i$ sites (Table S1 of the supplementary material). The Si–Si bond length in the "isolated" dumbbell is 2.502 Å at 6 GPa.

K_5Si_2. K_5Si_2 dominates the range of pressure from 6.5 GPa to 28.5 GPa, adopting R-$3m$ symmetry [Z = 1, Fig. 3(d)], in which Si atoms occupy the crystallographic $2c$ sites. The structural feature of R-$3m$-K_5Si_2 is identical to

R-$3m$-Li_5Si_2,[31] in which the silicon dumbbell (bond length, 2.389 Å at 9 GPa) is arranged along the c-axis. It is worth noting that a ratio of 5:2 is also favored in the Li–Sn[50] and Ca–C systems.[13] The results indicate that the component ratio of 5:2 is a favorable one for group IA-IVA or IIA-IVA compounds.

K_2Si. Triclinic P-1-K_2Si [Z = 4, Fig. 3(e)] stabilizes in a narrow pressure range of 12.5 GPa-12.8 GPa. Structurally, it includes zigzag Si_4 groups in which the bond lengths are 2.314 Å and 2.350 Å and the bond angle is about 125.81° at 2.5 GPa. Upon compression, the triclinic P-1-K_2Si transforms into an orthorhombic $Cmcm$-K_2Si [Z = 4, Fig. 3(f)] at 12.8 GPa. The Si atoms in the $Cmcm$-K_2Si phase are aggregated into zigzag chains. It is surprising that there is an abnormal extension in Si–Si bond length compared to the low-pressure P-1 phase. At 12.8 GPa, the bond length of Si–Si in silicon atomic chains is about 2.522 Å and the Si–Si–Si angle is 113.99°.

K_3Si_2. K_3Si_2 crystallizes in the P-1 structure [Z = 2, Fig. 3(g)] and is thermodynamically stable from 15 GPa to 27.5 GPa. Si atoms form a parallelogram with the bond lengths of 2.400 Å and 2.404 Å and the Si–Si–Si angle of 90.427° and 89.570° at 1.0 GPa.

KSi. KSi has three thermodynamically stable phases (P-$43n$, $I4_1/acd$, and $C2/c$). The well-known cubic P-$43n$-KSi[32] [Z = 32, Fig. 3(h)] is reproduced in our structure searches at ambient pressure. The optimized lattice parameter (12.733 Å) agrees well with the experimental data (12.620 Å).[32,33] Two nonequivalent Si atoms locate at the $24i$ (0.562, 0.073, 0.183) and $8e$ (0.568, 0.568, 0.568) sites, respectively. Si1 atoms form slightly distorted tetrahedrons with two different Si-Si bond lengths (2.428 Å and 2.447 Å) at ambient pressure, while Si2 atoms form regular tetrahedrons with a bond length of 2.435 Å at ambient pressure [see Fig. 4(h)]. We
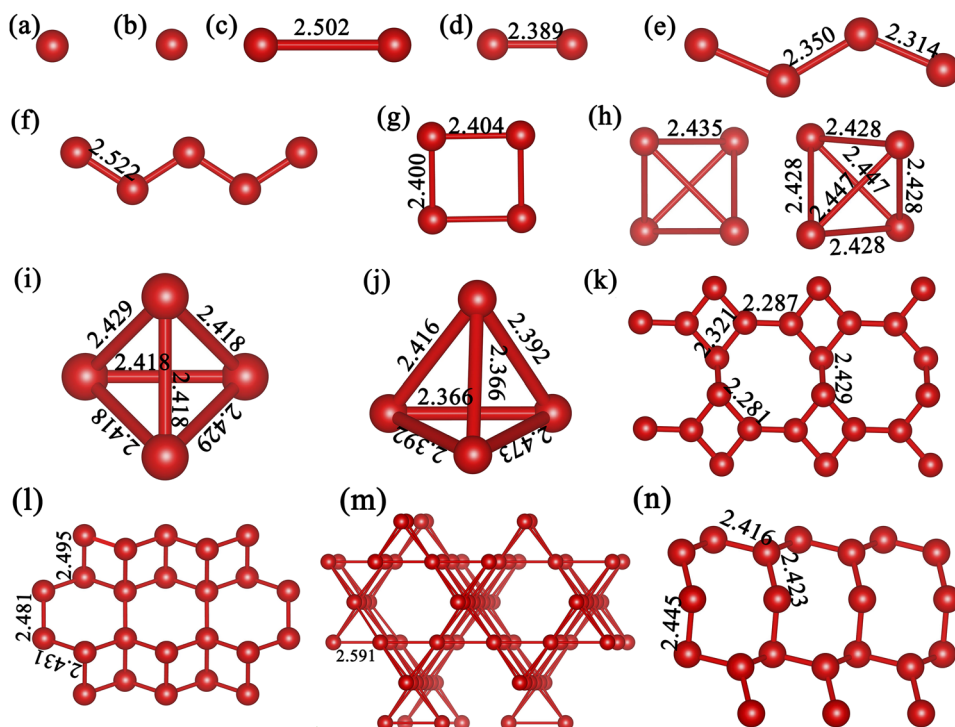

FIG. 4. Silicon patterns in the K–Si system at examined pressures. Bond length is in Å. (a) $I4/m$-K_4Si at 4 GPa, (b) R-$3m$-K_4Si at 16 GPa, (c) $C2/m$-K_3Si at 6 GPa, (d) R-$3m$-K_5Si_2 at 9.0 GPa, (e) P-1-K_2Si at 2.5 GPa, (f) $Cmcm$-K_2Si at 12.8 GPa, (g) P-1-K_3Si_2 at 1 GPa, (h) P-$43n$-KSi at 0 GPa, (i) $I4_1/acd$-KSi at 2.2 GPa, (j) $C2/c$-KSi at 11 GPa, (k) P-1-KSi at 24.5 GPa, (l) $C2/m$-KSi_2 at 5 GPa, (m) Fd-$3m$-KSi_2 at 18.5 GPa, and (n) $C2/m$-KSi_3 at 0 GPa.

performed some component-fixed calculations (at the selected pressure points of 5 GPa and 10 GPa) with the constraint that the number of K_4Si_4 in the unit cell is up to 4 formulas (that is, at most 32 atoms in the unit cell). It turns out that the NaPb-type structure was reproduced in our searching. The NaPb-type structure (space group $I4_1/acd$), with isolated Si_4 tetrahedra [Si–Si bond lengths are 2.418 Å and 2.429 Å, see Fig. 4(i)] surrounded by K atoms [see Fig. 3(i)], is thermo-dynamically stable at the pressure range from 2.2 GPa to 11 GPa. The predicted phase transition pressure of 2.2 GPa from P-43n phase to $I4_1/acd$ phase is in good agreement with the experimental data (about 4 GPa).[34] The tetragonal NaPb-type structure transformed into a monoclinic $C2/c$ structure at the pressure of 11 GPa, in which the silicon tetrahedrons (the mean Si–Si bond length is 2.401 Å) were kept [see Figs. 3(j) and 4(j)]. Thus, isolated silicon tetrahedra are still stable up to 24.5 GPa in the KSi compounds. Above 24.5 GPa, P-1-KSi (Z = 4) becomes thermodynamically metastable. It has an interesting layered structure consisting of alternating layers of K atoms and Si atoms [see Fig. 3(k)]. In the silicon layer, the 4-membered rings share a Si–Si bond with four neighbor congeners, constructing a "4 + 8"ring pattern, in which Si–Si bond lengths are between 2.281 Å and 2.429 Å at 24.5 GPa [see Figs. 3(k) and 4(k)].

KSi₂. The monoclinic $C2/m$-KSi₂ [Z = 4, Fig. 3(l)] is thermodynamically metastable at the range of pressure from 5.0 GPa to 18.5 GPa. Different from the silicon layer revealed in P-1-KSi, Si atoms in $C2/m$-KSi₂ polymerize into a novel layer structure, in which the neighbor silicon stripes with 4-membered rings are welded by the shared Si–Si bonds, presenting the wrinkled "4 + 6" ring pattern [the Si–Si bond lengths are between 2.431 Å and 2.495 Å at 5 GPa; see Fig. 4(l)]. Differing from the heavier congener KPb_2 with the hexagonal Laves phase $MgZn_2$-type structure[51] (space group $P6_3/mmc$, Z = 4) at ambient pressure, the thermodynamically stable KSi₂ crystallized in the cubic Laves phase $MgCu_2$-type structure[52] [space group Fd-3m, Z = 8, Fig. 3(m)] above 18.5 GPa. In the $MgCu_2$-type structure of KSi₂, silicon atoms aggregate into the three-dimensional framework structure with the K atoms running through the tunnels (structurally, K atoms form zigzag chains.). The neighboring silicon tetrahedrons are hinged by a shared silicon atom [six-fold coordinated silicon observed, Fig. 4(m)], constructing a strong covalent network and thus bringing about a strong incompressibility of this system. The pressure-induced structural modification from the monoclinic $C2/m$ structure to the cubic Fd-3m leads to a counter-intuitive chemical bond expansion phenomenon for Si-Si bonds. The Si-Si bond length in Fd-3m at 18.5 GPa is 2.591 Å, which is longer than that in the low-pressure $C2/m$-KSi₂.

KSi₃. The Si-rich $C2/m$-KSi₃ [Z = 4, Fig. 3(n)] is thermodynamically stable above 2.5 GPa (metastable below 2.5 GPa). Three inequivalent Si atoms locate at three 4i sites, forming a wrinkled two-dimension layer with silicon 8-membered rings. At zero pressure, the Si–Si bond length is between 2.416 Å and 2.445 Å [Fig. 4(n)].

K₈Si₄₆. The known cubic K₈Si₄₆ [space group Pm-3n, Z = 1, Fig. 3(o)] is thermodynamically stable below 17.5 GPa.

It belongs to cage-type structures composed of face-sharing silicon polyhedra of Si_{20} and Si_{24}, strictly analogous to the well-known gas or liquid hydrates, such as $8Cl_2 \cdot 46H_2O$.[36] Two small Si_{20} cages and six large Si_{24} cages offer the eight sites for guest K atoms.

C. Electronic properties

To understand the electronic properties of K-Si compounds predicted here, we calculated the electronic band structures and density of states (DOSs) (Fig. 5 and Figs. S4 and S5 of the supplementary material). In the Si-rich systems, all the structures are semiconductors, except for P-1-KSi and Fd-3m-KSi₂. At the K-rich side, all compounds predicted here exhibit some metallicity, except R-3m-K₄Si (an indirect gap of 0.68 eV) and P-1-K₃Si₂ (a direct gap of 0.59 eV).

From the DOS plots in Fig. 5, we can clearly see a strong hybridization of s, p, and d orbitals of K for all structures and also a hybridization between K orbitals and Si-p orbitals. This is a common feature shared by alkali metal compounds under high pressures. The semiconductivity or metallicity depends on the topology of Si sublattice and K:Si ratio. Due to a much larger electronegativity, Si gains electrons from K. The chemical bonding between Si and K is a mixture of covalency and iconicity, as shown by ELFs in Fig. S6 of the supplementary material. Between Si atoms, it is of covalent characteristic. In K-rich compounds, the Si sublattice needs more electrons from K besides the limited shared electrons between Si atoms themselves to fill its 3p orbitals; if filled like in R-3m-K₄Si, the compound shows semiconducting; otherwise like in $I4/m$-K₄Si, it will be metallic. And in K-rich compounds, most of them are metallic because the semiconductivity asks for an appropriate Si sublattice under a specific K:Si ratio, in order to completely fulfill Si-p orbitals and produce a closed-shell K. The same argument also applies to Si-rich compounds. However, in Si-rich environment, K can be easily stripped off electrons and surrounded by the Si sublattice with covalent character like $C2/m$-KSi₃. Therefore, most Si-rich compounds are semiconductors. Fd-3m-KSi₂ is metallic because a K–K bonding network exists between Si layers.

In the same stoichiometry, the electronic structure can be subjected to metal-semiconductor changes due to the structural evolution and reorganization. The P-43n-KSi, an indirect semiconductor with a bandgap of 1.24 eV at 0 GPa, first transforms into the semiconducting $I4_1/acd$-KSi at 2.2 GPa (an indirect bandgap of 1.31 eV) and then into the semiconducting $C2/c$ structure at 11 GPa (a direct bandgap of 1.48 eV). The $C2/c$-KSi transforms into the metallic P-1-KSi above 24.5 GPa. The $C2/m$-KSi₂ is a narrow gap semiconductor with an indirect bandgap of 0.23 eV at 5 GPa. Upon compression, the semiconducting $C2/m$-KSi₂ transforms into the metallic Fd-3m-KSi₂ at 18.5 GPa. The $C2/m$-KSi₃ holds an indirect bandgap of 0.80 eV at 0 GPa. There is also a metal-semiconductor transition in K₄Si, and similarly, such a transition was also observed in an isoelectronic compound Ca_2C.[13] Differing from the two-dimensional metallicity in the metallic phase of Ca_2C, $I4/m$-K₄Si is a semimetal due to a very small overlap between the bottom of the conduction band

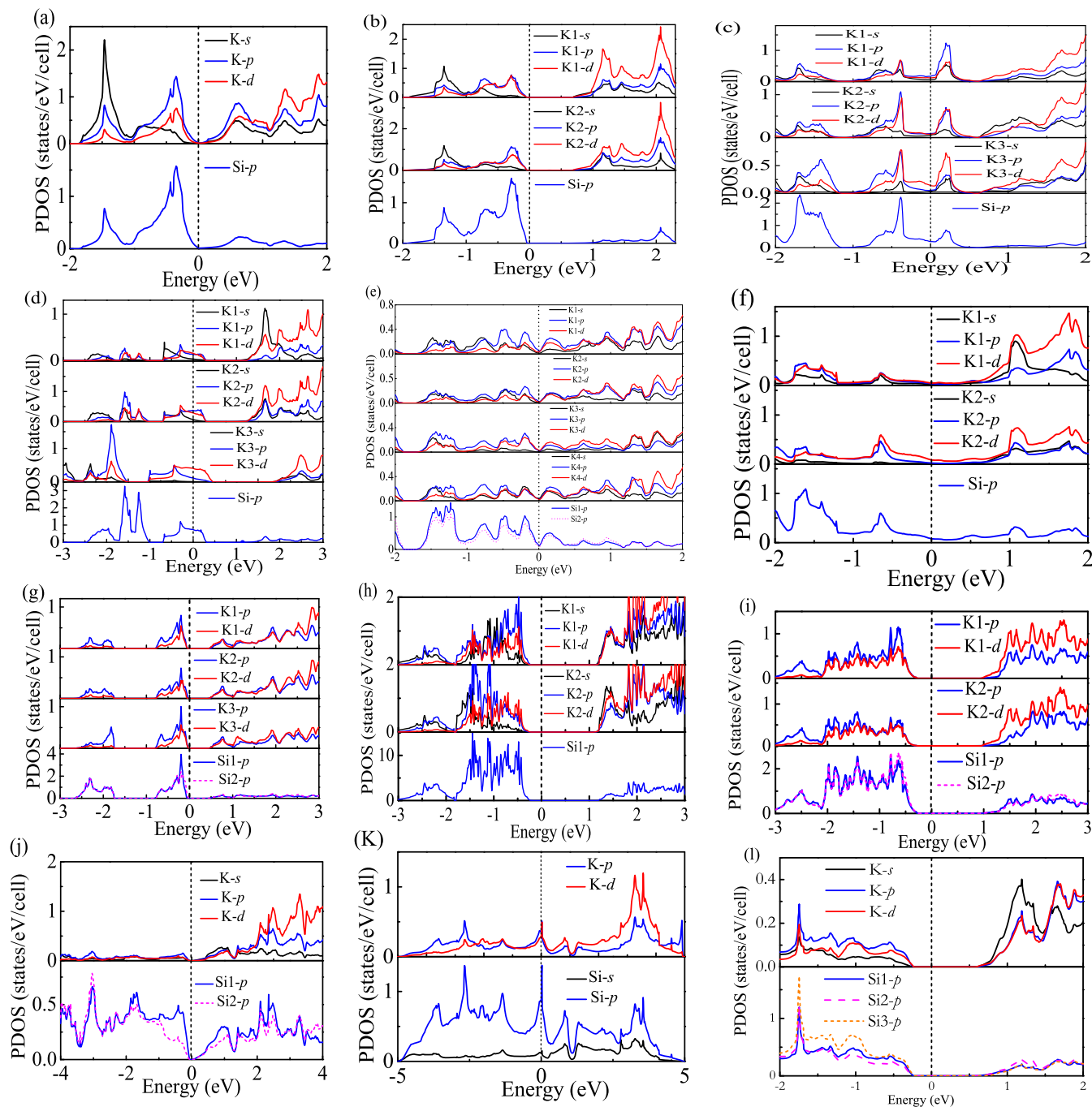FIG. 5. Projected density of states of (a) $I4/m$-K$_4$Si at 4 GPa, (b) R-3m-K$_4$Si at 16 GPa, (c) $C2/m$-K$_3$Si at 6 GPa, (d) R-3m-K$_5$Si$_2$ at 9.0 GPa, (e) P-1-K$_2$Si at 2.5 GPa, (f) $Cmcm$-K$_2$Si at 12.8 GPa, (g) P-1-K$_3$Si$_2$ at 1 GPa, (h) $I4_1/acd$-KSi at 2.2 GPa, (i) $C2/c$-KSi at 11 GPa, (j) $C2/m$-KSi$_2$ at 5 GPa, (k) Fd-3m-KSi$_2$ at 18.5 GPa, and (l) $C2/m$-KSi$_3$ at 0 GPa.

and the top of valence band. We also found that P-1-K$_2$Si is a semimetal.

ELF maps the likelihood of finding an electron in the neighborhood space of a reference electron. In order to understand the bonding nature between the atoms in the K–Si system, ELFs were calculated and shown in Fig. S6 of the supplementary material. One can conclude from ELF plots that all compounds predicted here show obvious ionic characteristics for K–Si bonding, which in nature attributes to the large difference of electronegativity between the K atom and Si atom. As Si content increases, we can see

the increasing ELF values between Si atoms that signal the strong covalent bonding. Different from the case of Ca-rich carbides in the Ca–C system,[13] there is no interstitial electron charge accumulation in the K-rich silicides predicted here, indicating that these K-rich compounds are not electrides.

To further explore the potential applications of novel semiconductors predicted here (R-3m-K$_4$Si, P-1-K$_3$Si$_2$, P-43n-KSi, $C2/m$-KSi$_2$, and $C2/m$-KSi$_3$), we calculated their dielectric properties. From the calculated dielectric functions, we can derive the optical absorption coefficients, which were
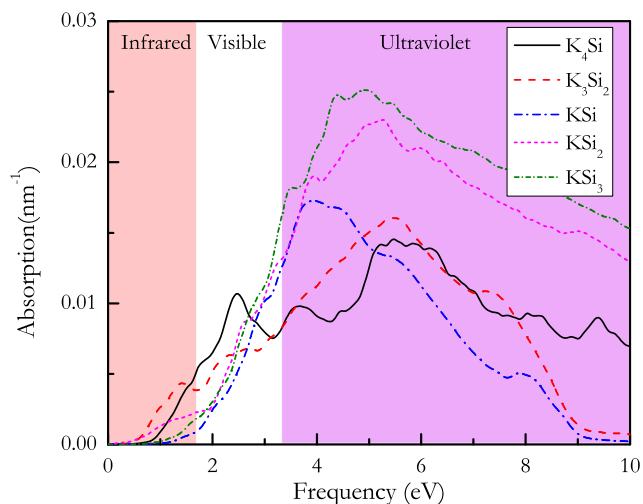
FIG. 6. The optical absorption spectrum of five semiconductors: R-$3m$-K_4Si, P-1-K_3Si_2, P-$43n$-KSi, $C2/m$-KSi_2, and $C2/m$-KSi_3.

plotted in Fig. 6. The five predicted compounds exhibit considerably stronger absorption than diamond silicon in the infrared and the visible light range. R-$3m$-K_4Si has a pronounced absorption peak around 2.5 eV, suggesting that this structure has potential applications in the visible light range.

IV. CONCLUSION

In summary, we have produced the first complete pressure-composition phase diagram for K–Si compounds at pressures up to 30 GPa by performing variable-composition evolutionary structure searching. The K–Si system holds a rich thermodynamic phase diagram and presents a strong structural diversity. Eight novel K–Si compounds were identified and their structural phase transition sequences were also determined. With the increasing Si content, the form of polymerization of silicon atoms has undergone great changes, from the zero dimensional "isolated" silicon anions to Si dimers to novel Si_4 group (zigzag, quadrangle, or tetrahedron) to one-dimensional chain to two-dimensional layers and to three-dimensional open structures, presenting dimensional diversity. For two-dimensional silicon layers, silicon exhibits various patterns including "4 + 8" rings, "4 + 6" rings, and 8-membered rings, which essentially depends on the K:Si ratio and external pressure so as to overcome the potential barrier. The structural diversity leads to various manifestations of electronic structures which depend on the form of Si polymerization and K:Si ratio. K–Si bonding shows a character of mixed covalency and iconicity, while Si–Si is of covalent character. Therefore, most compounds in the Si-rich side are semiconductors, except for the case when K forms its own bonding network. Semiconducting compounds can also form in the K-rich side only if the Si-p orbital is fulfilled and K is left with closed-shell orbitals, which needs simultaneously both an appropriate K:Si ratio and Si polymerization. The excellent optical absorption properties of semiconducting compounds predicted here will evoke their potential applications on the utilization of the solar energy. We believe that the revealed compounds

and chemistry in the K–Si system are useful for future studies and applications and that our findings will ignite further experimental and theoretical studies on alkali metal-based IVA compounds.

SUPPLEMENTARY MATERIAL

See supplementary material for the crystal structures' information, phonon dispersion curves, energy band, and electronic localization function of the studied K–Si system.

ACKNOWLEDGMENTS

[1] G. Profeta, M. Calandra, and F. Mauri, Nat. Phys. **8**, 131–134 (2012).
[2] D. Connétable, V. Timoshevskii, B. Masenelli, J. Beille, J. Marcus, and B. Marcus, Phys. Rev. Lett. **91**, 247001 (2003).
[3] D. Benson, Y. L. Li, W. Luo, R. Ahuja, G. Svensson, and U. Haussermann, Inorg. Chem. **52**, 6402–6406 (2013).
[4] Y. L. Li, W. Luo, Z. Zeng, H. Q. Lin, H. K. Mao, and R. Ahuja, Proc. Natl. Acad. Sci. U. S. A. **110**, 9289–9294 (2013).
[5] C. Zhang, J. Lan, H. Jiang, and Y. L. Li, J. Phys. Chem. C **120**, 10137–10145 (2016).
[6] D. Y. Kim, S. Stefanoski, O. O. Kurakevych, and T. A. Strobel, Nat. Mater. **14**, 169–173 (2015).
[7] M. Christensen, A. B. Abrahamsen, N. B. Christensen, F. Juranyi, N. H. Andersen, K. Lefmann, J. Andreasson, C. R. Bahl, and B. B. Iversen, Nat. Mater. **7**, 811–815 (2008).
[8] M. Zeilinger, I. M. Kurylyshyn, U. Häussermann, and T. F. Fässler, Chem. Mater. **25**, 4623–4632 (2013).
[9] Z. Zeng, Q. Zeng, N. Liu, A. R. Oganov, Q. Zeng, Y. Cui, and W. L. Mao, Adv. Energy Mater. **5**, 1500214 (2015).
[10] Y. Lin, T. A. Strobel, and R. E. Cohen, Phys. Rev. B **92**, 214106 (2015).
[11] Y. L. Li, W. Luo, X. J. Chen, Z. Zeng, and H. Q. Lin, Sci. Rep. **3**, 3331 (2013).
[12] Y. L. Li, R. Ahuja, and H. Q. Lin, Chin. Sci. Bull. **59**, 5269–5271 (2014).
[13] Y. L. Li, S. N. Wang, A. R. Oganov, H. Gou, J. S. Smith, and T. A. Strobel, Nat. Commun. **6**, 6974 (2015).
[14] L. Wang, X. Huang, D. Li, Y. Huang, K. Bao, F. Li, G. Wu, B. Liu, and T. Cui, J. Chem. Phys. **144**, 194506 (2016).
[15] H. Zheng, L. Wang, K. Li, Y. Yang, Y. Wang, J. Wu, X. Dong, C.-H. Wang, C. A. Tulk, J. J. Molaison, I. N. Ivanov, M. Feygenson, W. Yang, M. Guthrie, Y. Zhao, H.-K. Mao, and C. Jin, Chem. Sci. **8**, 298–304 (2017).
[16] X. Jiang, J. Zhao, Y. L. Li, and R. Ahuja, Adv. Funct. Mater. **23**, 5846–5853 (2013).
[17] J. Wu, H. Gao, K. Xia, D. Xing, and J. Sun, Appl. Phy. Lett. **111**, 173904 (2017).
[18] H. Sung, W. H. Han, I. Lee, and K. J. Chang, Phys. Rev. Lett. **120**, 157001 (2018).
[19] H. Okamoto, Bull. Alloy Phase Diagrams **11**, 306–312 (1990).
[20] M. H. Braga, A. Dębski, and W. Gąsior, J. Alloys Compd. **616**, 581–593 (2014).
[21] V. L. Chevrier, J. W. Zwanziger, and J. R. Dahn, J. Alloys Compd. **496**, 25–36 (2010).
[22] R. Nesper and H. G. V. Schnering, J. Solid State Chem. **70**, 48–57 (1987).
[23] A. Kuhn, P. Sreeraj, P. R. Pöttgen, M. Wilkening, and P. P. Heitjans, Angew. Chem., Int. Ed. **50**, 12099–12102 (2011).
[24] N. Artrith, A. Urban, and G. Ceder, J. Chem. Phys. **148**, 241711 (2018).
[25] U. Frank, W. Müller, and H. Schäfer, Z. Naturforsch. B **30**, 10–13 (1975).
[26] Y. Kubota, M. C. S. Escano, H. Nakanishi, and H. Kasai, J. Appl. Phys. **102**, 053704–053706 (2007).

[27] D. Thomas, M. Zeilinger, D. Gruner, R. Hüttl, J. Seidel, A. U. B. Wolter, T. F. Fässler, and F. Mertens, J. Chem. Thermodyn. **85**, 178–190 (2015).

[28] W. W. Tipton, C. R. Bealing, K. Mathew, and R. G. Hennig, Phys. Rev. B **87**, 184114 (2013).

[29] S. Zhang, Y. Wang, G. Yang, and Y. Ma, ACS Appl. Mater. Inter. **8**, 16761–16767 (2016).

[30] A. J. Morris, C. P. Grey, and C. J. Pickard, Phys. Rev. B **90**, 054111 (2014).

[31] I. Valencia-Jaime, R. Sarmiento-Pérez, S. Botti, M. A. L. Marques, M. Amsler, S. Goedecker, and A. H. Romero, J. Alloys Compd. **655**, 147–154 (2016).

[32] E. Busmann, Z. Anorg. Allg. Chem. **313**, 90–106 (1961).

[33] L. H. Yang, C. D. Consorte, C. Y. Fong, J. E. Pask, E. Nabighian, S. M. Kauzlarich, and J. S. Nelson, Chem. Mater. **10**, 4025–4029 (1998).

[34] J. Evers, G. Oehlinger, G. Sextl, and A. Weiss, Angew. Chem., Int. Ed. Engl. **23**, 528–529 (1984).

[35] V. Quéneau, E. Todorov, and S. C. Sevov, J. Am. Chem. Soc. **120**, 3263–3264 (1998).

[36] C. Cros, M. Pouchard, and P. Hagenmuller, J. Solid-State Chem. **2**, 570–581 (1970).

[37] J.-N. Chotard, W. S. Tang, P. Raybaud, and R. Janot, Chem. - Eur. J. **17**, 12302–12309 (2011).

[38] J. S. Tse, S. Desgreniers, Z. Q. Li, and Y. Kawazoe, Phys. Rev. Lett. **89**, 195507 (2002).

[39] T. Kume, T. Koda, S. Sasaki, H. Shimizu, and J. S. Tse, Phys. Rev. B **70**, 052101 (2004).

[40] W. Zhang, Z. Y. Zeng, N. N. Ge, and Z. G. Li, Materials **9**, 616 (2016).

[41] A. R. Oganov, A. O. Lyakhov, and M. Valle, Acc. Chem. Res. **44**, 227–237 (2011).

[42] A. O. Lyakhov, A. R. Oganov, H. T. Stokes, and Q. Zhu, Comput. Phys. Commun. **184**, 1172–1182 (2013).

[43] W. Zhang, A. R. Oganov, A. F. Goncharov, Q. Zhu, S. E. Boulfelfel, A. O. Lyakhov, E. Stavrou, M. Somayazulu, V. B. Prakapenka, and Z. Konôpková, Science **342**, 1502–1505 (2013).

[44] J. Hafner, Comput. Phys. Commun. **177**, 6–13 (2007).

[45] J. P. Perdew, K. Burke, and M. Ernzerhof, Phys. Rev. Lett. **77**, 3865–3868 (1996).

[46] A. Togo, F. Oba, and I. Tanaka, Phys. Rev. B **78**, 134106 (2008).

[47] K. Parlinski, Z. Q. Li, and Y. Kawazoe, Phys. Rev. Lett. **78**, 4063–4066 (1997).

[48] P. Giannozzi, S. Baroni, N. Bonini, M. Calandra, R. Car, C. Cavazzoni, D. Ceresoli, G. L. Chiarotti, M. Cococcioni, I. Dabo, A. Dal Corso, S. de Gironcoli, S. Fabris, G. Fratesi, R. Gebauer, U. Gerstmann, C. Gougoussis, A. Kokalj, M. Lazzeri, L. Martin-Samos, N. Marzari, F. Mauri, R. Mazzarello, S. Paolini, A. Pasquarello, L. Paulatto, C. Sbraccia, S. Scandolo, G. Sclauzero, A. P. Seitsonen, A. Smogunov, P. Umari, and R. M. Wentzcovitch, J. Phys. Condens. Matter. **21**, 395502 (2009).

[49] A. D. Becke and K. E. Edgecombe, J. Chem. Phys. **92**, 5397–5403 (1990).

[50] U. Frank, W. Müller, and H. Schäfer, Z. Naturforsch. B **30**, 1–5 (1975).

[51] D. Gilde, Z. Anorg. Allg. Chem. **284**, 142–143 (1956).

[52] J. B. Friauf, J. Am. Chem. Soc. **49**, 3107–3114 (1927).